J. Fluid Mech. (2001), *vol.* 442, *pp.* 161–170. Printed in the United Kingdom

Passive scalar anisotropy in a heated turbulent wake: new observations and implications for large-eddy simulations

By HYUNG SUK KANG AND CHARLES MENEVEAU

Department of Mechanical Engineering, Johns Hopkins University, 3400 North Charles Street, Baltimore, MD 21218, USA

(Received 24 March 2001 and in revised form 22 May 2001)

The effects of passive scalar anisotropy on subgrid-scale (SGS) physics and modelling for large-eddy simulations are studied experimentally. Measurements are performed across a moderate Reynolds number wake flow generated by a heated cylinder, using an array of four X-wire and four cold-wire probes. By varying the separation distance among probes in the array, we obtain filtered and subgrid quantities at three different filter sizes. We compute several terms that comprise the subgrid dissipation tensor of kinetic energy and scalar variance and test for isotropic behaviour, as a function of filter scale. We find that whereas the kinetic energy dissipation tensor tends towards isotropy at small scales, the SGS scalar-variance dissipation remains anisotropic independent of filter scale. The eddy-diffusion model predicts isotropic behaviour, whereas the nonlinear (or tensor eddy diffusivity) model reproduces the correct trends, but overestimates the level of scalar dissipation anisotropy. These results provide some support for so-called mixed models but raise new questions about the causes of the observed anisotropy.

1. Introduction

The statistics and general structure of passive scalars in turbulent flows differ significantly from those of the turbulent velocity field. In particular, conclusive experimental (e.g. Stewart 1969; Sreenivasan, Antonia & Britz 1979; Mestayer 1982; Mydlarski & Warhaft 1998*a*) and numerical (e.g. Holzer & Siggia 1994) evidence shows that structure functions and the derivative skewness of the scalar field do not follow predictions from isotropy at inertial and dissipative scales, in the presence of a mean scalar gradient. In particular, the deviations are thought to be related to 'ramp and cliff structures' and to imply a direct effect of large-scale structures on small-scale structures. The data relevant to this question have been reviewed by Sreenivasan (1991) and more recently by Warhaft (2000). Moreover, scalar spectra display a distinctly less universal structure than velocity spectra. This is manifested in terms of both spectral exponents and the dimensionless spectral coefficient c_θ. The latter varies from values near 0.4 in many experiments in the atmospheric surface layer and grid turbulence (see Sreenivasan 1991, 1996 and Warhaft 2000) to $c_\theta \sim 1.8$ for other atmospheric measurements (Antonia *et al.* 1997 and Antonia, Xu & Zhou 1999). From a fundamental point of view, these observations challenge the Kolmogorov cascade phenomenology for the transfer of scalar variance from large to small scales. In the classical phenomenology, the multiplicity of separate 'eddy breakdown' events is assumed to gradually uncouple the small from the large scales, allowing the former

to tend to a universal and isotropic structure more or less independent of the large scales. On the contrary, the scalar-field measurements suggest a direct linkage among largest and smallest scales.

The coupling among scales is an important ingredient in large-eddy simulations (LES). In LES, the turbulent fields (velocity and scalar) are decomposed into large and small (subgrid-scale, SGS) scale contributions by means of a spatial low-pass filter of characteristic width Δ. The resulting equations which can be numerically discretized with mesh spacing of the order of Δ require closure of the unresolved momentum fluxes (SGS stress tensor, $\tau_{ij} \equiv \widetilde{u_i u_j} - \widetilde{u}_i \widetilde{u}_j$, where a tilde represents filtering at scale Δ) and scalar fluxes (e.g. the SGS heat flux, $q_j \equiv \widetilde{\theta u_j} - \widetilde{\theta}\widetilde{u}_j$ where θ is the passive scalar field). The promise of LES is often predicated upon small-scale universality and isotropy, and the absence of a strong coupling across disparate length scales. Hence, the observed anisotropy of the scalar field seems to pose a challenge to the very foundation of LES. While these deviations from classical phenomenology are now quite well established, little is known about their impact on the closure problem for LES. The present work quantifies the implications of small-scale scalar anisotropy on quantities that describe subgrid-scale physics and directly affect modelling for LES.

As reviewed in Meneveau & Katz (2000), the most important statistical property of the fluxes τ_{ij} and q_j is how they affect the mean kinetic energy and scalar-variance budgets of the resolved fields. Specifically, their dominant effect is through the kinetic energy and scalar-variance dissipations that arise from interactions between subgrid and resolved scales. Therefore, in the present study, we mainly focus on the so-called SGS kinetic energy dissipation $-\langle \tau_{ij}\widetilde{S}_{ij}\rangle$ (Piomelli *et al.* 1991) and scalar-variance dissipation $-\langle q_j \widetilde{G}_j\rangle$ (Porté-Agel, Meneveau & Parlange 1998). Here $\widetilde{S}_{ij} \equiv \frac{1}{2}\left(\partial\widetilde{u}_i/\partial x_j + \partial\widetilde{u}_j/\partial x_i\right)$ and $\widetilde{G}_j \equiv \partial\widetilde{\theta}/\partial x_j$ are the resolved strain-rate tensor and scalar gradient, respectively. The SGS dissipation rates represent the flux (cascade) of kinetic energy or scalar-variance from resolved towards subgrid scales (when positive). When Δ pertains to the inertial range, and when the flow is in equilibrium, one expects the mean SGS dissipation to equal the molecular dissipation rate.

Deviations from isotropy in the context of SGS dissipation can be probed by measuring the isotropy level of the tensors $-\langle \tau_{ij}\widetilde{S}_{mn}\rangle$ and $-\langle q_i \widetilde{G}_j\rangle$, as a function of scale. The main question to be addressed in this work is whether the approach to isotropy (if it exists) is the same for kinetic energy and scalar-variance dissipation tensors. Another goal is to test the ability of two popular model classes (eddy diffusivity and nonlinear models, see Meneveau & Katz 2000 for a review) to reproduce the observations. In order to span a sizeable range of inertial-range filter scales, a sufficiently high Reynolds number must be considered. Hence, this study is based on experimental data (as opposed to DNS which is limited to small Reynolds numbers). The study is performed in a canonical shear flow, the heated cylinder wake.

2. Experiment apparatus and flow characteristics

Experiments were performed in the return type Corrsin Wind Tunnel (Comte-Bellot & Corrsin 1966). A heated smooth cylinder of diameter $D = 4.83\,\text{cm}$ was located horizontally at the centreline of the test section. The measurement location in the streamwise direction (x_1) was fixed at $x_1/D = 25$. To obtain the filtered and SGS quantities, an array of four custom-made miniature probes was used. Each probe was composed of one X-type hot wire and one I-type cold wire for the velocities in the

(x_1, x_2)-plane and the temperatures, respectively. Here x_2 is the 'cross-wake' direction, i.e. perpendicular to x_1 and to the cylinder axis.

The separation distance h between the probes in the cross-wake direction x_2 could be adjusted manually between 5 and 20 mm. Three configurations ($\Delta = 2h$, with $h = 5$, 10 and 20 mm) were used in the present study. A 2.5 μm platinum-coated tungsten wire which had been copper-plated was soldered on to the X-wire prong ends and etched, yielding an active length-to-diameter ratio of about 200. The wire spacing between the hot wires was 0.5 mm. A 0.625 μm silver-coated pure platinum wire for a cold-wire sensor was soldered on the I-wire prong ends and subsequently etched. To minimize the low-frequency amplitude attenuation, the active length-to-diameter ratio was about 1000 as suggested by Bruun (1995). The separation distance between the cold wire and its nearest hot wire was 0.9 mm so that the thermal effect from the hot wire on the cold wire was negligible. The signals were low-pass filtered at a frequency of 20 kHz and sampled at $f_s = 40$ kHz. Sampling time was 60 s, so the total number of data points per channel for each measurement location was 2.4×10^6. The array was traversed across the wake, and data were recorded at 17 discrete cross-wake locations from the centreline to the wake edge at increments of 14.4 mm.

At the measurement location of $x_1/D = 25$, the mean centreline velocity (U_{CL}) was 13.6 m s^{-1}, the defect velocity ($U_d = U_\infty - U_{CL}$) was 4.4 m s^{-1}, the defect temperature ($\theta_d = \theta_{CL} - \theta_\infty$) was 0.61 °C, and the half-width of the wake was $\ell = 0.08$ m. To get the spatial quantities along the streamwise direction from the temporal data, Taylor's hypothesis was invoked. The turbulence intensity of the streamwise velocity at the centreline was about 13.3%. The molecular kinetic energy dissipation at the centreline (ϵ_{CL}) was 87 m^2 s^{-3}, and the molecular scalar-variance dissipation at the centreline ($\epsilon_{\theta CL}$) was 0.65 °C^2 s^{-1}. The latter two variables were obtained from (corrected) third-order structure functions as in Cerutti, Meneveau & Knio (2000) and Lindborg (1999). It follows that the Kolmogorov length scale ($\eta = (\nu^3/\epsilon)^{1/4}$) was 0.08 mm, the Taylor microscale (λ) was 2.9 mm, and the Reynolds number based on Taylor microscale (Re_λ) was 350. The longitudinal integral scale obtained by integrating up to the first zero crossing of the u_1 correlation function was $L_{11} = 0.091$ m. Profiles of mean velocity, r.m.s. velocities, Reynolds shear stress, r.m.s. temperature and heat flux distributions across the wake agreed quite well with results in the literature (e.g. Matsumura & Antonia 1993 and Kiya & Matsumura 1988).

In the present study, to separate large and small scales the box filter is applied to the streamwise and cross-wake directions, and the trapezoidal rule is used for the spatial integrations. The filtering process consists in a discrete approximation to a two-dimensional box filter. In the x_2-direction, a four-point discretization is used for evaluating the SGS fluxes while a three-point approximation is used for the filtered derivatives. Filtered velocity and scalar gradients in the x_2-direction are evaluated using first-order finite differences over a distance h. In the streamwise direction, the box filter is approximated using $\Delta f_s/\langle u_1 \rangle$ sampling points and the x_1-derivatives are evaluated using finite differences over a distance h. The filtering and error analysis is documented in Cerutti & Meneveau (2000) and Cerutti *et al.* (2000).

Figure 1(*a*) shows a comparison between the longitudinal spectrum $E_{11}(\kappa_1)$ of the u_1-component and the longitudinal spectrum $E_{22}(\kappa_1)$ of the u_2-component multiplied by 3/4 at the centreline. Here, κ_1 is the longitudinal wavenumber. The three vertical lines correspond to the filter sizes of $\Delta/\eta = 125$ (10 mm), 250 (20 mm), 500 (40 mm). All the filter sizes are in the inertial range. Since the noise peak in the longitudinal spectrum of u_1 is in the far dissipation region, quite removed from any of the filter frequencies and scales of interest in this study, no effort is made to remove the noise

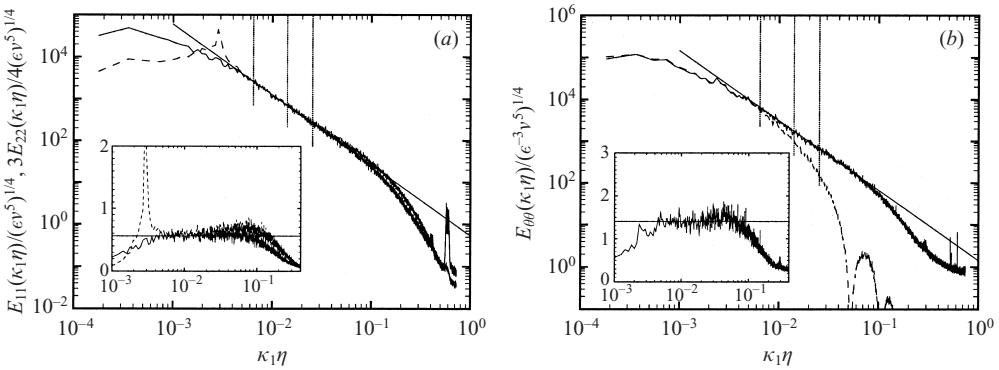

FIGURE 1. Velocity and temperature spectra at the centreline, in Kolmogorov units. (*a*) The longitudinal spectrum of the u_1-component (solid line) and of the u_2-component multiplied by 3/4 (dashed line), as a function of the longitudinal wavenumber, κ_1. The spectrum of u_2 is below that of u_1 at low wavenumber ($\kappa_1\eta < 0.002$) with a Strouhal peak ($\kappa_1\eta \sim 0.003$), and higher at high wavenumber ($0.1 < \kappa_1\eta < 0.4$). (*b*) The longitudinal spectrum of the temperature (solid line) and of the temperature, filtered at $\Delta/\eta = 125$ (dashed line). The inserts in (*a*) and (*b*) show the compensated spectra, $E_{11}(\kappa_1)\,\epsilon^{-2/3}\kappa_1^{5/3}$, $\frac{3}{4}E_{22}(\kappa_1)\,\epsilon^{-2/3}\kappa_1^{5/3}$ and $E_{\theta\theta}(\kappa_1)\,\epsilon_\theta^{-1}\epsilon^{1/3}\kappa_1^{5/3}$. The three vertical lines are the wavenumbers corresponding to the filter sizes of $\Delta/\eta = 125$ (10 mm), 250 (20 mm), 500 (40 mm). The straight sloping solid lines are the universal spectra (see text).

by additional filtering (various attempts such as notch filtering showed no effect on the results). It can be clearly observed that $E_{11}(\kappa_1) \approx \frac{3}{4}E_{22}(\kappa_1)$ as required by isotropy in the inertial range, over about one decade of wavenumbers. The peak in $E_{22}(\kappa_1)$ at $\kappa_1\eta \sim 0.003$ is due to the periodic von Kármán vortex street behind the cylinder. The frequency of the vortices is 78.1 Hz, and this gives Strouhal number $S_t\ (= fD/U_\infty) = 0.211$. The Kolmogorov constant c_K in $E_{11}(\kappa_1) = \frac{18}{55}c_K\epsilon^{2/3}\kappa_1^{-5/3}$ is obtained as $c_K = \frac{55}{18}(0.56) = 1.71$ in the insert. This value is quite close to the standard value of 1.6 (see Sreenivasan 1995) and a similar value of 1.7 was observed by O'Neil & Meneveau (1997). Figure 1(*b*) shows the longitudinal spectrum of the temperature $E_{\theta\theta}(\kappa_1)$. As seen in the compensated spectrum shown in the insert, there is a fairly clear inertial range with a $-5/3$ slope. This slope is steeper than those found in the round jet by Tong & Warhaft (1995) and Miller & Dimotakis (1996), and in several other shear flows reviewed in Sreenivasan (1996). It is closer to results quoted in Antonia & Pearson (1997), who report a scaling exponent of 0.65–0.66 for the second-order temperature structure function in the heated cylinder wake at $Re_\lambda = 230$, or to the spectra for grid turbulence of Mydlarski & Warhaft (1998*b*).

The coefficient c_θ in $E_{\theta\theta}(\kappa_1) = c_\theta\epsilon_\theta\epsilon^{-1/3}\kappa_1^{-5/3}$ deduced from this spectrum is about 1.4. It is significantly higher than results quoted in Sreenivasan (1996) for high Reynolds numbers, but is within the range of results from various shear flow measurements reported in Antonia *et al.* (1999). As discussed in Sreenivasan (1996), the dissipation measurements are based on assuming scalar isotropy and are thus subject to considerable uncertainty. On the other hand, at the centreline we find good isotropy (see § 3) which would seem to support our current estimates of the dissipation and c_θ. While the universality of c_θ and spectral exponent is not the main subject of this paper, the scatter of results certainly supports the view that the scalar spectrum for shear flows at moderate Reynolds numbers (e.g. $Re_\lambda < 1000$) depends upon details of the generation of the flow (Sreenivasan 1996). Specifically, it seems that the dependence of the spectral exponent and prefactor on Re_λ is not universal.

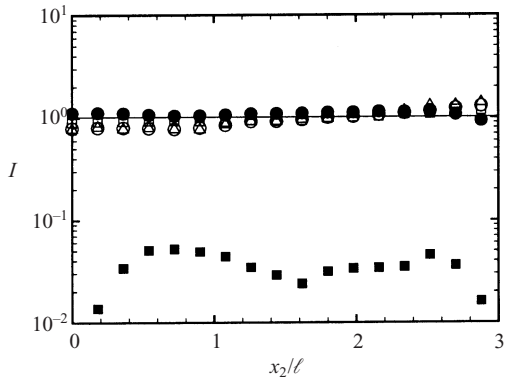

FIGURE 2. Isotropy ratios of the filtered gradient fields and of the mean SGS stresses across the heated wake at $x_1/D = 25$ with the filter size of $\Delta/\eta = 125$: ○, $\langle\widetilde{S}_{22}\widetilde{S}_{22}\rangle/\langle\widetilde{S}_{11}\widetilde{S}_{11}\rangle$; □, $\langle\widetilde{S}_{12}\widetilde{S}_{12}\rangle/\langle\frac{3}{4}\widetilde{S}_{11}\widetilde{S}_{11}\rangle$; △, $\langle\widetilde{G}_2\widetilde{G}_2\rangle/\langle\widetilde{G}_1\widetilde{G}_1\rangle$; ●, $\langle\tau_{22}\rangle/\langle\tau_{11}\rangle$; ■, $-\langle\tau_{12}\rangle/\langle\tau_{11}\rangle$.

The longitudinal spectrum of the filtered temperature is shown as the dashed curve in figure 1(*b*). The lobes at scales below the filter size are due to the streamwise box filter used in the present study. Spectra of filtered velocity (not shown) have a similar shape.

3. Isotropy of real SGS dissipation and model predictions

In discussing isotropy of various tensors, we distinguish second-rank and fourth-rank tensors. Examples of second-rank tensors are the mean SGS stress $\langle\tau_{ij}\rangle$, the filtered scalar gradient $\langle\widetilde{G}_i\widetilde{G}_j\rangle$, and the SGS scalar-variance dissipation $-\langle q_i\widetilde{G}_j\rangle$. Their isotropic form can be written as $\langle\tau_{ij}\rangle = \langle\tau_{11}\rangle\delta_{ij}$, $\langle\widetilde{G}_i\widetilde{G}_j\rangle = \langle\widetilde{G}_1\widetilde{G}_1\rangle\delta_{ij}$, and $\langle q_i\widetilde{G}_j\rangle = \langle q_1\widetilde{G}_1\rangle\delta_{ij}$ respectively. On the other hand, the strain-rate-product tensor $\langle\widetilde{S}_{ij}\widetilde{S}_{pq}\rangle$ and SGS dissipation tensor $\langle\tau_{ij}\widetilde{S}_{pq}\rangle$ are fourth-rank tensors. Their isotropic form can be written as

$$\langle\tau_{ij}\widetilde{S}_{pq}\rangle = -\tfrac{1}{2}\langle\tau_{11}\widetilde{S}_{11}\rangle[\delta_{ij}\delta_{pq} - \tfrac{3}{2}\left(\delta_{ip}\delta_{jq} + \delta_{iq}\delta_{jp}\right)], \tag{1}$$

and a similar expression holds for $\langle\widetilde{S}_{ij}\widetilde{S}_{pq}\rangle$ by replacing τ_{ij} with $\widetilde{S}_{ij}$. To derive the above expression, we have used the tensor symmetry (in $i-j$ or $p-q$) and the divergence-free condition ($\widetilde{S}_{kk} = 0$). It follows that $\langle\widetilde{S}_{22}\widetilde{S}_{22}\rangle = \langle\widetilde{S}_{11}\widetilde{S}_{11}\rangle$ and $\langle\widetilde{S}_{12}\widetilde{S}_{12}\rangle = \frac{3}{4}\langle\widetilde{S}_{11}\widetilde{S}_{11}\rangle$.

Figure 2 shows isotropy ratios of the filtered gradient fields and of the mean SGS stresses, for $\Delta/\eta = 125$. In isotropic conditions, all ratios have to be on the unit line except $\langle\tau_{12}\rangle/\langle\tau_{11}\rangle$ which should tend to zero with decreasing filter scale since the fraction of mean shear stress carried by the SGS is expected to vanish when $\Delta/\ell \to 0$. As can be seen, both the SGS stress and strain-rate fields are quite isotropic across the heated wake flow at this scale. For the larger filter sizes of $\Delta/\eta = 250$ and 500 (not shown), the trends are similar to figure 2 but slightly less isotropic.

Next, results are given for the SGS dissipation tensors across the wake. We define the following 'isotropy ratios':

$$I_{u22} \equiv \frac{\langle\tau_{22}\widetilde{S}_{22}\rangle}{\langle\tau_{11}\widetilde{S}_{11}\rangle}, \quad I_{u12} \equiv \frac{\langle\tau_{12}\widetilde{S}_{12}\rangle}{\frac{3}{4}\langle\tau_{11}\widetilde{S}_{11}\rangle}, \quad I_\theta \equiv \frac{\langle q_2\widetilde{G}_2\rangle}{\langle q_1\widetilde{G}_1\rangle}. \tag{2}$$

Figures 3(*a*) and 3(*b*) show the spatial distributions of the SGS kinetic energy

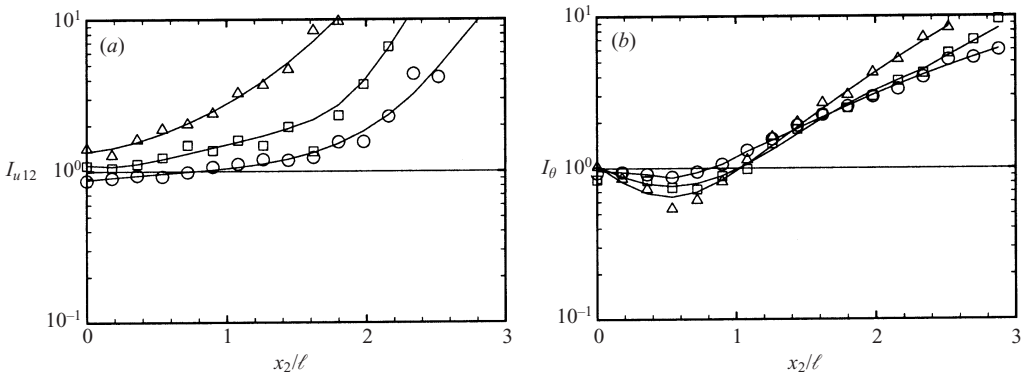

FIGURE 3. Isotropy ratios in the SGS dissipations: (*a*) I_{u12}; (*b*) I_θ (see (2)): ○, $\Delta/\eta = 125$; □, $\Delta/\eta = 250$; △, $\Delta/\eta = 500$. For clarity, fourth-order polynomial fits of $\log I$ vs. x_2/ℓ are added as solid lines.

dissipation isotropy ratios I_{u12} and the SGS scalar-variance dissipation isotropy ratios I_θ, respectively, across the wake flow with the different filter sizes. All moments in this study are statistically well converged. For example, running averages such as $n^{-1}\sum_{k=1}^{n} q_i\tilde{G}_j$ did not differ from their global average by more than 6% over the last 80% of data (i.e. for $n \in [0.2N, N]$ where $N = 2.4 \times 10^6$). For different filter sizes considered, the SGS kinetic energy and scalar-variance dissipations are isotropic only towards the centreline of the wake. Towards the edges of the wake, large anisotropies persist (even though there the mean shear and mean temperature gradients vanish also). The isotropy ratio of I_{u12} at a fixed x_2/ℓ in figure 3(*a*) clearly increases with the filter size. However, the isotropy ratio of the scalar-variance dissipation I_θ shows almost no variation with filter size for $1 < x_2/\ell < 2$, where the scalar gradient in the cross-wake direction, $\partial\theta/\partial x_2$, is large.

The increased anisotropy in the outer regions of the wake (see figure 3*a*, *b*) is another striking result. The anisotropy may be associated with the highly intermittent character of the flow there. One may wonder whether the anisotropy arises from a superposition of distinct behaviours in the turbulent and the non-turbulent (outer) regions. Using conditional averaging, O'Neil & Meneveau (1997) have showed that the conditional averages of the SGS dissipations in the non-turbulent regions were negligible compared to those in the turbulent regions. The implication was that the global averages of dissipation could be explained entirely by their conditional mean value inside the turbulent part: $\langle\tau_{ij}\tilde{S}_{ij}\rangle \approx \Gamma\langle\tau_{ij}\tilde{S}_{ij}\rangle_T$, where $\Gamma(x_2)$ is the intermittency function (i.e. the fraction of time the signal is turbulent at any given x_2), and the subscript T stands for averaging conditioned on 'turbulence' (see O'Neil & Meneveau 1997 for details). When replacing the conditional averages multiplied by Γ in the expression for isotropy ratios, Γ cancels from both numerator and denominator. This behaviour suggests that the anisotropy ratios shown in figure 3 are equal to those inside the turbulent regions alone, and that their rise in the outer parts of the wake cannot be explained by contributions from the non-turbulent parts. However, it is still possible that non-trivial contributions to the scalar-variance dissipations could originate at the interface separating turbulent from non-turbulent regions.

To highlight the variations with filter scale more directly, in figure 4 we plot the isotropy ratios as a function of scale, for the transverse location $x_2/\ell = 1.44$ close to the peak mean temperature gradient. As is evident, the isotropy ratios of the kinetic energy dissipation decrease towards unity as the filter size decreases, whereas the

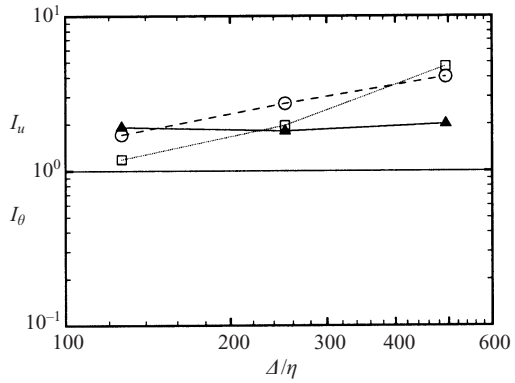

FIGURE 4. Isotropy ratios of kinetic energy and scalar-variance SGS dissipations at $x_2/\ell = 1.44$, where the mean temperature gradient peaks. The open symbols (and dashed and dotted lines) represent isotropy ratios for the SGS dissipation of kinetic energy: ○, I_{u22}; and □, I_{u12}; the closed triangles ▲ (and solid line) are for the scalar dissipation I_θ.

isotropy ratio of the scalar-variance dissipation remains unchanged near $I_\theta \sim 2$ as the filter size is decreased. As seen in figure 3, near the centreline, where the mean shear and scalar gradient vanish, the SGS isotropy ratios are all near unity.

Therefore, we conclude that in terms of the most important of the resolved-SGS interactions (the mean SGS dissipation), the scalar field maintains strong anisotropy in the presence of a mean scalar gradient. Conversely, the velocity field has the trends expected from approach to isotropy at small scales.

Next, we quantify the isotropy level of model predictions, when the data are analysed in an *a priori* sense, i.e. by replacing τ_{ij} and q_j above by model expressions. First, the standard eddy-diffusion model is considered, i.e.

$$\tau_{ij}^{\mathrm{Smag}} - \tfrac{1}{3}\tau_{kk}^{\mathrm{Smag}}\delta_{ij} = -2(C_S\Delta)^2|\widetilde{S}|\widetilde{S}_{ij}, \quad q_j^{\mathrm{Smag}} = -2Pr_{\mathrm{sgs}}^{-1}(C_S\Delta)^2|\widetilde{S}|\widetilde{G}_j, \tag{3}$$

where $|\widetilde{S}| = \left(2\widetilde{S}_{mn}\widetilde{S}_{mn}\right)^{1/2}$ is the modulus of the resolved strain rate, C_S is the Smagorinsky coefficient, and Pr_{sgs} is the SGS Prandtl number. Consequently, and independent of the model coefficients, the isotropy ratios from the eddy-diffusion model are

$$I_{u22}^{\mathrm{Smag}} \equiv \frac{\langle|\widetilde{S}|\widetilde{S}_{22}\widetilde{S}_{22}\rangle}{\langle|\widetilde{S}|\widetilde{S}_{11}\widetilde{S}_{11}\rangle}, \quad I_{u12}^{\mathrm{Smag}} \equiv \frac{\langle|\widetilde{S}|\widetilde{S}_{12}\widetilde{S}_{12}\rangle}{\frac{3}{4}\langle|\widetilde{S}|\widetilde{S}_{11}\widetilde{S}_{11}\rangle}, \quad I_\theta^{\mathrm{Smag}} \equiv \frac{\langle|\widetilde{S}|\widetilde{G}_2\widetilde{G}_2\rangle}{\langle|\widetilde{S}|\widetilde{G}_1\widetilde{G}_1\rangle}. \tag{4}$$

In computing the filtered strain-rate magnitude from the data, the following approximation is used (this is a two-dimensional extension of the one-dimensional approach of O'Neil & Meneveau 1997, and was also used in Liu, Katz & Meneveau 1999): $|\widetilde{S}| \approx [2(2\widetilde{S}_{11}\widetilde{S}_{11} + \widetilde{S}_{22}\widetilde{S}_{22} + 6\widetilde{S}_{12}\widetilde{S}_{12})]^{1/2}$. This approximation is not expected to affect the accuracy of our measured isotropy ratios significantly. The reason is that $|\widetilde{S}|$ and its two-dimensional approximation are scalars which multiply equally all terms of the squared velocity and scalar gradients and is further supported by the isotropic behaviour of second-order moments of $\widetilde{S}_{ij}$ shown in figure 2. The isotropy ratios of the SGS dissipations from the eddy-diffusion model are shown in figure 5(*a*). Results are near unity almost independently of scale, including the passive scalar dissipation. Profiles across the wake (not shown) also are near unity. This result is consistent with the observed isotropy of the square gradient tensors shown in figure 2 (the only difference here is the additional $|\widetilde{S}|$ factor). Hence, using the eddy-diffusion model one would (incorrectly) predict SGS isotropy since the resolved second-order moments are isotropic.

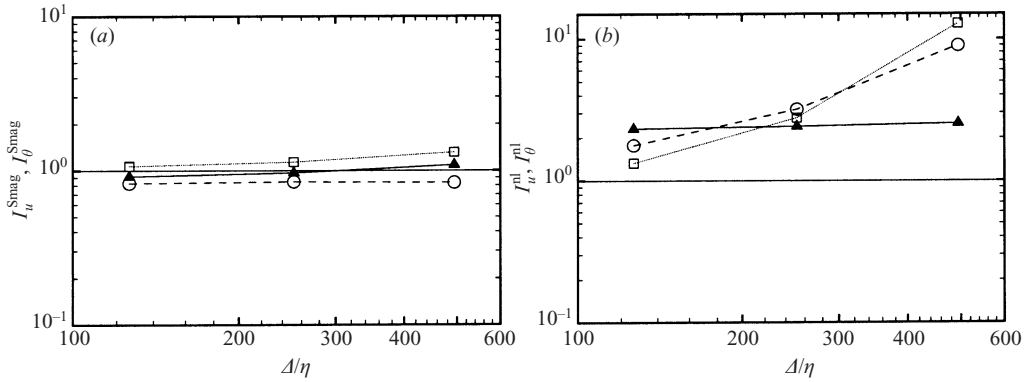

FIGURE 5. Isotropy ratios of components in SGS dissipations from models at $x_2/\ell = 1.44$, as a function of filter scale: (*a*) eddy-diffusion models: ○, I_{u22}^{Smag}; □, I_{u12}^{Smag}; ▲, I_θ^{Smag} (see (4)); (*b*) nonlinear models: ○, I_{u22}^{nl}; □, I_{u12}^{nl}; ▲, I_θ^{nl} (see (6)).

The second modelling class to be considered here is the 'nonlinear model' or 'tensor eddy-diffusion model' (Leonard 1974, 1977; Clark, Ferziger & Reynolds 1979; Liu, Meneveau & Katz 1994; Borue & Orszag 1998; Meneveau & Katz 2000). The nonlinear model reads as follows:

$$\tau_{ij}^{\mathrm{nl}} = C_{nl}\Delta^2 \frac{\partial \widetilde{u}_i}{\partial x_k}\frac{\partial \widetilde{u}_j}{\partial x_k}, \quad q_j^{\mathrm{nl}} = C_{nl_\theta}\Delta^2 \frac{\partial \widetilde{\theta}}{\partial x_k}\frac{\partial \widetilde{u}_j}{\partial x_k}, \tag{5}$$

where C_{nl} and C_{nl_θ} are the nonlinear model coefficients. Therefore, the corresponding isotropy ratios from the nonlinear model are defined as follows:

$$I_{u22}^{\mathrm{nl}} \equiv \frac{\left\langle \frac{\partial \widetilde{u}_2}{\partial x_k}\frac{\partial \widetilde{u}_2}{\partial x_k}\widetilde{S}_{22}\right\rangle}{\left\langle \frac{\partial \widetilde{u}_1}{\partial x_k}\frac{\partial \widetilde{u}_1}{\partial x_k}\widetilde{S}_{11}\right\rangle}, \quad I_{u12}^{\mathrm{nl}} \equiv \frac{\left\langle \frac{\partial \widetilde{u}_1}{\partial x_k}\frac{\partial \widetilde{u}_2}{\partial x_k}\widetilde{S}_{12}\right\rangle}{\frac{3}{4}\left\langle \frac{\partial \widetilde{u}_1}{\partial x_k}\frac{\partial \widetilde{u}_1}{\partial x_k}\widetilde{S}_{11}\right\rangle}, \quad I_\theta^{\mathrm{nl}} \equiv \frac{\left\langle \frac{\partial \widetilde{\theta}}{\partial x_k}\frac{\partial \widetilde{u}_2}{\partial x_k}\widetilde{G}_2\right\rangle}{\left\langle \frac{\partial \widetilde{\theta}}{\partial x_k}\frac{\partial \widetilde{u}_1}{\partial x_k}\widetilde{G}_1\right\rangle}, \tag{6}$$

where k varies from 1 to 2 in the analysis of our two-dimensional data.

The isotropy ratios of the SGS dissipations from the nonlinear model are shown in figure 5(*b*), as a function of filter scale. As is apparent on comparing with figure 4, the main features of anisotropy and filter-size dependence are correctly reproduced qualitatively. Quantitatively, the levels of anisotropy are overestimated. For instance, the level of anisotropy for the modelled SGS scalar-variance dissipation appears to stay near $I_\theta^{\mathrm{nl}} \sim 2.5$ as opposed to $I_\theta \sim 2$ for the real SGS scalar dissipation.

4. Summary and conclusions

In studying passive scalar statistics in a turbulent shear flow with a mean temperature gradient we focus on statistics of interest to subgrid modelling and large-eddy simulation. In order to obtain the filtered and subgrid velocities and temperatures, a probe array composed of four X-wire and four cold-wire sensors is used and two-dimensional box filtering in the streamwise and cross-wake directions is applied to the data. The isotropy ratios of the SGS kinetic energy and scalar-variance dissipations are investigated as functions of position in the flow and of filter scale. Both dissipations are isotropic independent of filter size near the centreline where there is no mean shear or scalar gradient. However, at locations with high gradient (and also further towards the outer wake regions), we find that the scalar-variance dissipation remains highly anisotropic, independent of filter size. Conversely, the kinetic energy

dissipation tensor approaches isotropy as the filter size is decreased. A mechanistic explanation of the observed trends in terms of possible orientations of ramp and cliff structures is not evident to us at this time. The persistence of scalar anisotropy even at small scales is consistent with prior results for structure functions and gradient statistics of unfiltered turbulence (Mestayer 1982; Sreenivasan 1991; Warhaft 2000). The present results quantify the impact of this anisotropy on the interactions among large and small scales in the context of SGS modelling and LES.

We find that the predictions of eddy-diffusion models are much more isotropic than the real phenomenon. This may at first glance seem obvious since eddy-diffusion models are often invoked under the banner of isotropy. However, the present result does not arise from an explicit isotropy assumption built into the model, but because the resolved gradients have second-order statistics that are isotropic. For instance, if the scalar gradient tensor $\langle \tilde{G}_i \tilde{G}_j \rangle$ had been found to be anisotropic, it would have implied anisotropic behaviour of the eddy-diffusion model's predictions. Instead, the isotropy that exists in the filtered scalar gradients is incorrectly applied to model the anisotropic statistics of the SGS heat flux. The main problem for the eddy-diffusion model appears to be that it uses second-order statistics to model third-order statistics. Conversely, the anisotropy exists in the third-order moments that arise from the velocity and scalar product (q_i) multiplied by the scalar gradient ($\widetilde{G}_j$), but is not discernible in the second-order statistics of $\widetilde{G}_j$ alone (even when modulated by the strain-rate magnitude). The anisotropy is clearly discernible, however, in the third-order moments consisting of the filtered velocity gradients times scalar gradients squared that arise in the expression for modelled SGS dissipation of scalar variance using the nonlinear model. These expressions are able to reproduce the detailed phase relationships among the velocity and scalar field that govern the SGS dissipation (cascade) of scalar variance. We remark that the overprediction of anisotropy by the nonlinear model (and its underprediction by the eddy-diffusion model) is reminiscent of the opposing trends of these two models documented in Liu *et al.* (1999) for rapidly strained turbulence in cold flow. The opposing trends suggest that a linear combination of the two models, i.e. the 'mixed model', can be tuned to reproduce the correct amount of anisotropy (for a discussion of the application of mixed models in LES, see Meneveau & Katz 2000). However, note that the data for I_{u12} and I_{u22} at $\Delta/\eta = 250$ and 125 do not provide clear justification for choosing the mixed over the nonlinear model.

Finally, it is stressed that our results are obtained in a single flow for a single moderate Reynolds number. Even if the present evidence in figure 4 of an essentially scale-independent anisotropy for the scalar dissipation appears to be quite strong, the results could change in another flow, or at higher Reynolds numbers (we recall that according to Sreenivasan 1996, universal behaviour for the scalar requires Re_λ above 1000 or so). These considerations serve as motivation for further work in this area.

We thank Professors Z. Warhaft and L. Mydlarski for useful comments and suggestions about the cold-wire calibration. This work was financially supported by the National Science Foundation (grant CTS-9803385).

REFERENCES

Antonia, R. A., Ould-Rouis, M., Anselmet, F. & Zhu, Y. 1997 Analogy between predictions of Kolmogorov and Yaglom. *J. Fluid Mech.* **332**, 395–409.

Antonia, R. A. & Pearson, B. R. 1997 Scaling exponents for turbulent velocity and temperature increments. *Europhys. Lett.* **40**, 123–128.

Antonia, R. A., Xu, G. & Zhou, T. 1999 Reynolds number dependence of low-order turbulent temperature structure functions. *Europhys. Lett*. **48**, 43–48.

Borue, V. & Orszag, S. 1998 Local energy flux and subgrid-scale statistics in three-dimensional turbulence. *J. Fluid Mech.* **366**, 1–31.

Bruun, H. H. 1995 *Hot-Wire Anemometry*, pp. 144–45. Oxford University Press.

Cerutti, S. & Meneveau, C. 2000 Statistics of filtered velocity in grid and wake turbulence. *Phys. Fluids* **12**, 1143–1165.

Cerutti, S., Meneveau, C. & Knio, O. M. 2000 Spectral and hyper eddy viscosity in high-Reynolds-number turbulence. *J. Fluid Mech.* **421**, 307–338.

Clark, R. G., Ferziger, J. H. & Reynolds, W. C. 1979 Evaluation of subgrid models using an accurately simulated turbulent flow. *J. Fluid Mech.* **91**, 1–16.

Comte-Bellot, G. & Corrsin, S. 1966 The use of a contraction to improve the isotropy of grid generated turbulence. *J. Fluid Mech.* **25**, 657–682.

Holzer, M. & Siggia, E. D. 1994 Turbulent mixing of a passive scalar. *Phys. Fluids* **6**, 1820–1837.

Kiya, M. & Matsumura, M. 1988 Incoherent turbulent structure in the near wake of a normal plate. *J. Fluid Mech.* **190**, 343–356.

Leonard, A. 1974 Energy cascade in large-eddy simulations of turbulent fluid flows. *Adv. Geophys.* **18**, 237–248.

Leonard, A. 1997 Large-eddy simulation of chaotic convection and beyond. *Am. Inst. Aeronaut. Astronaut. Paper* 97-0204: 1–8.

Lindborg, E. 1999 Correction to the four-fifths law due to variations of the dissipation. *Phys. Fluids* **11**, 510–512.

Liu, S., Katz, J. & Meneveau, C. 1999 Evolution and modelling of subgrid scales during rapid straining of turbulence. *J. Fluid Mech.* **387**, 281–320.

Liu, S., Meneveau, C. & Katz, J. 1994 On the properties of similarity subgrid-scale models as deduced from measurements in a turbulent jet. *J. Fluid Mech.* **275**, 83–119.

Matsumura, M. & Antonia, R. A. 1993 Momentum and heat transport in the turbulent intermediate wake of a circular cylinder. *J. Fluid Mech.* **250**, 651–668.

Meneveau, C. & Katz, J. 2000 Scale-invariance and turbulence models for large-eddy simulation. *Ann. Rev. Fluid Mech.* **32**, 1–32.

Mestayer, P. 1982 Local isotropy and anisotropy in a high-Reynolds-number turbulent boundary layer. *J. Fluid Mech.* **125**, 475–503.

Miller, P. L. & Dimotakis, P. E. 1995 Measurements of scalar power spectra in high Schmidt number turbulent jets. *J. Fluid Mech.* **308**, 129–146.

Mydlarski, L. & Warhaft, Z. 1998*a* Three-point statistics and the anisotropy of a turbulent passive scalar. *Phys. Fluids* **10**, 2885–2894.

Mydlarski, L. & Warhaft, Z. 1998*b* Passive scalar statistics in high-Péclet-number grid turbulence. *J. Fluid Mech.* **358**, 135–175.

O'Neil, J. & Meneveau, C. 1997 Subgrid-scale stresses and their modelling in a turbulent plane wake. *J. Fluid Mech.* **349**, 253–293.

Piomelli, U., Cabot, W., Moin, P. & Lee, S. 1991 Subgrid-scale backscatter in turbulent and transitional flows. *Phys. Fluids* A **3**, 1766.

Porté-Agel, F., Meneveau, C. & Parlange, M. B. 1998 Some basic properties of the surrogate subgrid-scale heat flux in the atmospheric boundary layer. *Boundary-Layer Met*. **88**, 425–444.

Sreenivasan, K. R. 1991 On the local isotropy of passive scalars in turbulent shear flows. *Proc. R. Soc. Lond*. A **434**, 165–182.

Sreenivasan, K. R. 1995 On the universality of the Kolmogorov constant. *Phys. Fluids* **7**, 2778–2784.

Sreenivasan, K. R. 1996 The passive scalar spectrum and the Obukhov-Corrsin constant. *Phys. Fluids* **8**, 189–196.

Sreenivasan, K. R., Antonia, R. A. & Britz, D. 1979 Local isotropy and large structures in a heated turbulent jet. *J. Fluid Mech.* **94**, 745–775.

Stewart, R. W. 1969 Turbulence and waves in stratified atmosphere. *Radio Sci.* **4**, 1269–1278.

Tong, C. & Warhaft, Z. 1995 Passive scalar dispersion and mixing in a turbulent jet. *J. Fluid Mech.* **292**, 1–38.

Warhaft, Z. 2000 Passive scalars in turbulent flows. *Ann. Rev. Fluid Mech.* **32**, 203–240.